# EROSIVE WEAR OF SELECTED MATERIALS FOR FOSSIL ENERGY APPLICATIONS

**Thomas A. Adler, James C. Rawers, Joseph H. Tylczak, and Jeffrey A. Hawk**
**U.S. Department of Energy**
**Albany Research Center**
**Albany, OR 97321**

## ABSTRACT

A number of materials have been evaluated to determine their erosion resistance for fossil energy applications. This is part of a larger program to study wear and corrosion at Albany Research Center. This paper will present the results for some of these materials, including FeAl, FeAl cermets, WC-Co cemented carbides, $Si_3N_4$-$MoSi_2$, $Si_3N_4$, Stellite 6B, white cast irons and 440C steel. Trends in erosion rates due to material properties and erosive conditions will be presented. FeAl cermets performed well compared to the WC-Co cemented carbides. The interparticle spacing of the WC-Co cemented carbides correlated with the erosion rate. The erosion rate of the WC-Co cemented carbides decreased as the interparticle spacing decreased. It is important to realize that erosion resistance is not an intrinsic material property, but is a system response. A change in the wear environment can significantly alter the relative rankings of materials with respect to their wear rate. For example, at relatively low velocities, the carbides in the white cast irons are more erosion resistant than the matrix, while at higher velocities the matrix is more erosion resistant.

## INTRODUCTION

Solid particle erosion both at room temperature and at elevated temperature is a significant problem in fossil energy plants.[1–3] Material wastage due to erosion and the combined effects of erosion and corrosion limit the lifetime of many parts such as pumps, valves, burner nozzles, heat exchanger tubes, and turbine blades. The Albany Research Center is conducting a program to identify the mechanism of erosion and corrosion under conditions that simulate fossil energy plants, and to identify materials that are resistant to erosion and corrosion.

## EXPERIMENTAL

FeAl-matrix cermets were produced at Oak Ridge National Laboratory (ONRL) by pressureless melt-infiltration of powder preforms. $TiB_2$, TiC and WC powders were cold-pressed into preforms (approximately 25 mm in diameter). The preforms were infiltrated by liquid FeAl (Fe-24 w/o Al which is equivalent to Fe-40 a/o Al) at 1450°C in a vacuum. Complete details on the processing can be found elsewhere.[4–8] For comparison to the FeAl-matrix cermets, conventional WC-6 w/o Co cemented carbides were obtained from a commercial vendor. This composition corresponds to Co-90 v/o WC. The microstructure of these cermets varied in WC grain size, ranging from 0.55 to 1.51 μm.

An FeAl alloy was also prepared for erosion testing.[9] This alloy was prepared by hot-pressing a mixture of the Fe-28 Al-5 Cr (composition in atomic %) powders with an appropriate amount of elemental Al powder to the base composition to produce an FeAl alloy consisting of Fe-49.5Al-1.25Cr.

An $Si_3N_4$-$MoSi_2$ composite was fabricated at the NASA Lewis Research Center from $MoSi_2$ and $Si_3N_4$ powders using a combination hot-pressing and hot isostatic pressing. Complete details on this composite

can be found in previous publications.[10–12] The erosion behavior of the composite was compared to that of monolithic β-$Si_3N_4$ samples, WC-6% Co samples and Stellite 6B (Co-28Cr-4W-3Mo w/o) samples from commercial vendors.

Hypoeutectic, eutectic and hypereutectic high-Cr white cast irons were produced by melting in an induction furnace and casting in sand molds. The composition (w/o) of the hypereutectic white cast iron was 3.66 C, 26.0 Cr, 0.79 Si, 0.22 Ni, 0.92 Mn, 0.30 Mo and balance Fe. Details of the sample preparation were given in previous publications.[13,14]

The cast steels with TiC reinforcements used in this work were melted in a vacuum induction furnace. The compositions and details of the sample preparation were given in a previous publication.[15] An AISI 440C steel and eight commercially available TiC particle reinforced P/M composites were used as comparison materials. The cast steels and the 440C steel were tested in both the as cast and heat treated conditions.

The gas jet erosion test followed ASTM G76-95 (ref. 16). The abrasive used was 50 μm alumina powder with a particle feed rate of 2 g/min. The carrier gas was commercial grade nitrogen gas and the abrasive was mixed with the gas in a commercial mixing device. The mixture was delivered through a 1.5 mm inner diameter tungsten carbide nozzle where the stream was ejected against the target material. The distance between the end of the nozzle and the target was 10 mm and the impingement angle was 90° for the room temperature tests. The particle velocity was 40 m/s for the majority of the tests as determined by a double disk calibration technique. A few test were run at 70 and 140 m/s. The gas flow rate was adjusted to maintain the desired particle velocity. The test times were 20 minutes for 40 m/s, 10 minutes for 70 m/s and 100 s for 140 m/s. For elevated temperature tests, the samples were enclosed in a heated test chamber. The carrier gas was 99.999% nitrogen for all tests performed at or above 500°C, and the impingement angle was 75°.

## RESULTS AND DISCUSSIONS

Figures 1 and 2 show the erosion rates as a function of temperature for the different WC-Co cemented carbides and the FeAl cermets.[4] Figure 1 shows that the erosion rates of the WC-Co cemented carbides increases with increasing carbide grain size. This carbide grain size effect on erosion behavior is consistent with that seen by other research,[17–23] and illustrates the dependency of erosion behavior on various microstructural features of the cemented carbides. Generally, for high carbide volume fractions, the erosion rate increases as the mean free path of the Co binder increases.[17–22] This trend correlates with an increase in the fracture toughness and a decrease in hardness as the mean free path of the Co binder increases.[20]

Erosion resistance of the FeAl cermets proceeds in the following way: the most wear resistant (i.e., the cermet with the lowest erosion rate) FeAl-80 v/o WC > FeAl-40 v/o $TiB_2$ > FeAl-80 v/o TiC the least wear resistant (i.e., the one that possessed the highest erosion rate.). The erosion resistance of cermets depends on a complex combination of material hardness and fracture toughness of both the hard reinforcing phase and the metal binder.[17–24] The properties of the eroding particles (such as hardness, size, fracture toughness, and density) and the velocity of the particles also play a significant role in the erosion rate.[17–20,25–27] The FeAl-80 v/o WC cermet contained a higher volume fraction of hard, erosion resistant reinforcing phase than did the FeAl-40 v/o $TiB_2$ cermet (Fig. 2). In this case, the FeAl-80 v/o WC cermet was harder and more erosion resistant than the FeAl-40 v/o $TiB_2$ cermet. The FeAl-40 v/o $TiB_2$ cermet performed better than the FeAl-80 v/o TiC cermet even though the FeAl-80 v/o TiC cermet was harder and contained a higher volume fraction of hard reinforcement. In fact, the FeAl-80 v/o TiC cermet was the hardest of all the FeAl cermets, and yet was the least wear resistant. This behavior can be explained

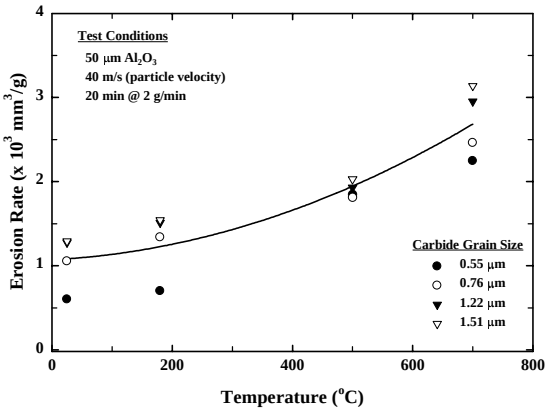


**Fig. 1. Erosion rate as a function of test temperature for WC-6w/oCo cemented carbides of various carbide sizes.**

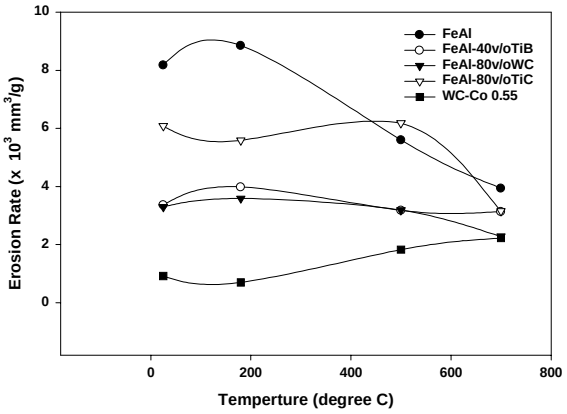


**Fig. 2. Erosion rate as a function of test temperature for FeAl and FeAl cermets.**

through examination of the microstructure, and by evaluation of the mechanism by which material was removed from the surface during erosion.

The damage in the erosion crater of the FeAl-80 v/o WC cermet is very similar in appearance to the damage of the conventional WC-Co cemented carbide (compare Figs. 3 and 4).[4] Material is worn from the FeAl-80 v/o WC and WC-Co surfaces by chipping and cracking of the carbide particles and through the normal process of ductile erosion of the binder. During erosion of the FeAl-40 v/o $TiB_2$ cermet, on the other hand, the FeAl matrix is preferentially worn, thereby exposing the $TiB_2$ particles (Fig. 5). In this case, the $Al_2O_3$ erodent particles were sufficiently small compared to the $TiB_2$ particle network to allow for preferential wear of the FeAl binder. The microstructural features of the FeAl-WC cermet and the WC-Co cemented carbide were of such a scale to prevent preferential FeAl and Co binder wear.

The morphological features of the damage in the erosion crater of the FeAl-TiC cermet appear much different than the damage in the FeAl-WC cermet and WC-Co cemented carbide (compare Fig. 6 to Figs. 3 and 4).[4] The FeAl-TiC cermet contained relatively coarse (i.e., greater than 10 μm in diameter) TiC particles. The TiC particles were easily fractured during erosion, where evidence of cleavage fracture is clearly visible in the erosion crater. Apparently, the fracture toughness of the TiC is much less than the WC or $TiB_2$.

Examination of Figs. 1 and 2 reveal that the erosion rates of the Fe-Al cermets tend to decrease (FeAl-WC, FeAl-TiC) or remain constant (FeAl-$TiB_2$) with increasing temperature, whereas, the erosion rates of the WC-Co cemented carbides continually increase with increasing test temperature.[4] At temperatures less than 700°C, the WC-Co cemented carbides were significantly more resistant to particle erosion than the FeAl-cermets. This was expected, because the WC-Co cemented carbides contain a higher volume fraction of carbide particles, and thus smaller interparticle spacing than the FeAl-cermets. However, at 700°C, the erosion resistance of the FeAl-$TiB_2$ and FeAl-TiC cermets was equivalent to that of the course (1.51 μm) carbide WC-Co cemented carbide. The erosion resistance of the FeAl-WC cermet was approximately 33% lower than the course WC-Co cemented carbide, and equivalent to the fine (0.55 μm) WC-Co material.

One potential reason for these trends may be related to the relative oxidation resistance of the respected materials, specifically the binders. Although the erosion tests were performed using a nitrogen carrier gas

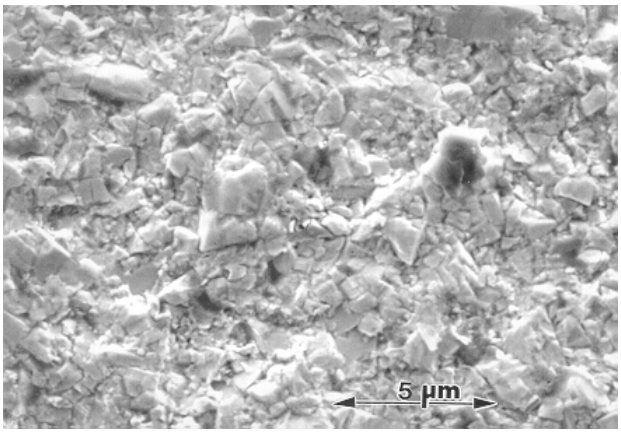


**Fig. 3. Erosion damage inside the erosion crater of WC-6v/oCo after testing at room temperature.**

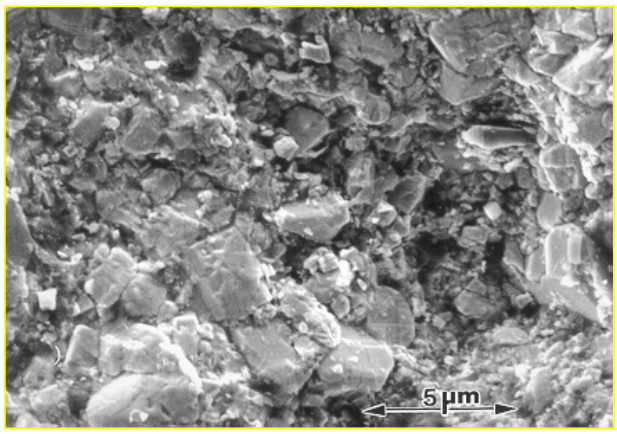


**Fig. 4. Erosion damage inside the erosion crater of FeAl-80v/oWC after testing at room temperature.**

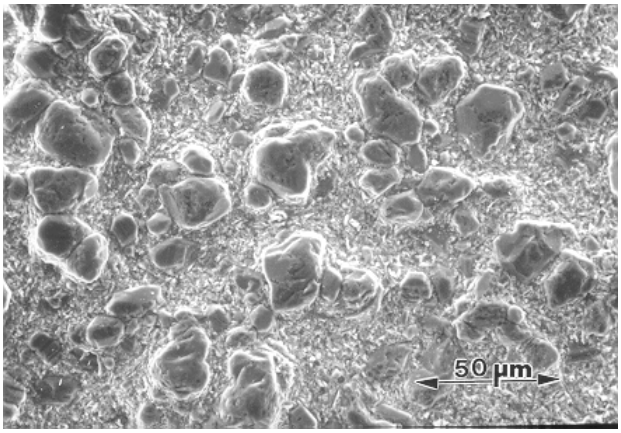


**Fig. 5. Erosion damage inside the erosion crater of FeAl-40v/o $TiB_2$ after testing at room temperature.**

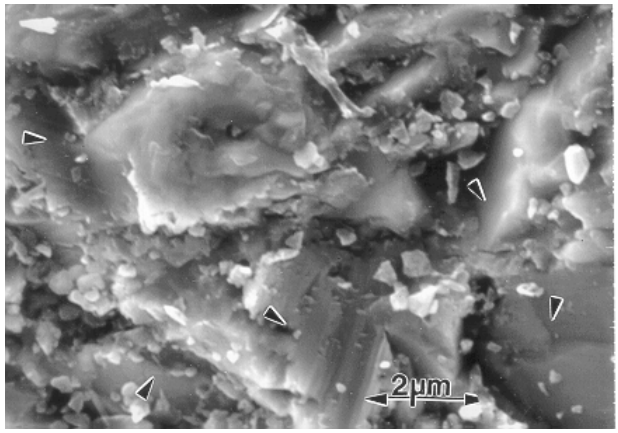


**Fig. 6. Erosion damage inside the erosion crater of FeAl-80v/oTiC after testing at room temperature.** The arrows point to cracks in the TiC.

in a furnace backfilled with nitrogen prior to testing, the nitrogen carrier gas contains some residual oxygen and the test chamber is not completely sealed to the ambient environment. Consequently, the specimens experience a mild oxidative environment. Specimens exposed to the nitrogen gas stream at 700°C without $Al_2O_3$ gained weight from oxidation.[4] The WC-Co alloys gained significantly more weight than the FeAl-cermets. Thus, the FeAl binder of the FeAl-cermets provides more oxidation protection than the Co binder of the WC-Co cemented carbides. During erosion, the formation of the oxide products on the surface can significantly affect erosion resistance. Typically, an oxide is brittle, and usually is more easily removed during erosion than the non-oxidized carbide. It appears that oxidation did not degrade the erosion resistance of the FeAl-cermets at the temperatures used in this study. Other mechanical factors, such as the influence of temperature on hardness, on interfacial strength between binder and the hard particle, and on fracture resistance may also contribute to the erosion behavior of these materials, but these specific mechanisms have not been studied to date.

Also shown in Fig. 2 are the erosion rates for a FeAl alloy.[9] At low temperatures (less than 500°C), the FeAl alloy had the highest erosion rate. However, at elevated temperature the FeAl alloy had a large drop

in erosion rate. The measured erosion rate for FeAl alloy at 700°C was approximately half of the erosion rate for this alloy at room temperature. It is not uncommon for the erosion rates of metals and alloys to decrease with increasing temperature in this temperature range.[2,3]

Figure 7 shows the erosion rates of the $Si_3N_4$-$MoSi_2$ composite, $Si_3N_4$ and Stellite-6B.[10] The measured erosion rate for Stellite-6B decreased slightly as the test temperature increased. This was similar to the trends for the FeAl-cermets discussed above. The erosion rate for the $Si_3N_4$-$MoSi_2$ composite remains relatively constant from room temperature to 700°C. The erosion rate decreased at 900°C. This decrease may be a result of a softening of the $MoSi_2$ phase at 900°C. However, there also was a drop in the erosion rate of the $Si_3N_4$ at 700°C. The erosion rate of the $Si_3N_4$ increased from 180 to 500°C, then decreased from 500 to 700°C. Scanning electron photomicrographs show the erosion damage in the wear scars of the $Si_3N_4$-$MoSi_2$ composite and $Si_3N_4$.[10] Material is removed by a brittle fracture mechanism, where cracks are formed as a result of particle impact and subsequently coalesce and intersect under the surface, as shown in Fig. 8. The damage appears similar for both the $Si_3N_4$-$MoSi_2$ composite and $Si_3N_4$.

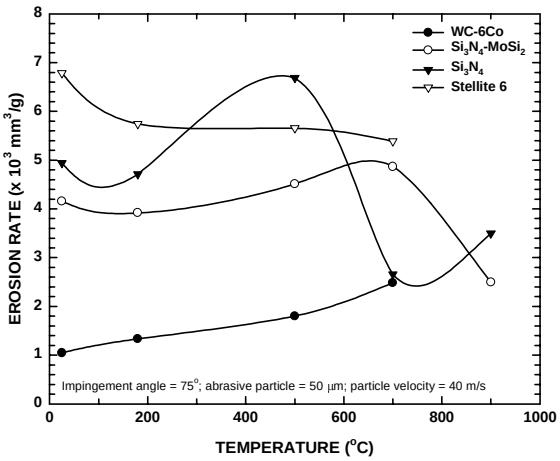


**Fig. 7. Erosion rate as a function of test temperature for $Si_3N_4$-$MoSi_2$, $Si_3N_4$, WC-Co, and Stellite 6B.**

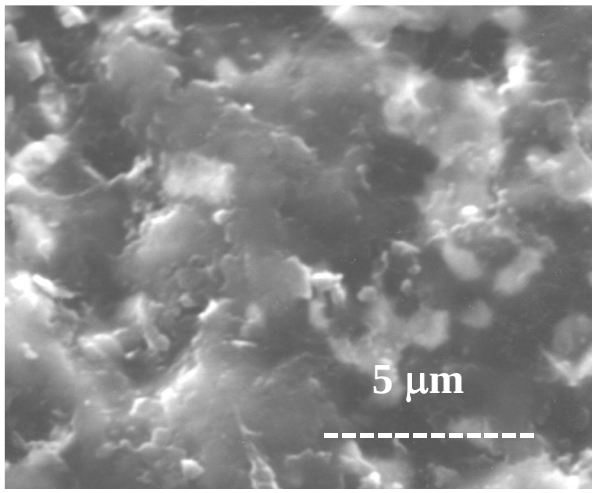


**Fig. 8. Erosion damage inside the erosion crater of $Si_3N_4$-$MoSi_2$ after testing at room temperature.**

The erosion rates of the white cast irons eroded by the alumina particles in the jet erosion test are shown in Fig. 9 (ref. 14). The erosion rate increased as a function of the particle velocity. The erosion rate did not change significantly with carbide content at 40 and 70 m/s. At 140 m/s the hypereutectic white cast iron had a higher erosion rate than the other two white cast irons. The appearance of the surface of the hypereutectic white cast iron eroded by the alumina is shown Figs. 10 and 11. For the hypereutectic white cast iron eroded at 40 and 70 m/s, the primary carbides protrude from the surface relative to the eutectic matrix (Fig. 10). While at 140 m/s, the primary carbides are recessed relative to the eutectic matrix (Fig. 11). In all cases, the erosion appeared to have occurred by a ductile processed on both the primary carbides and the eutectic matrix. The impact craters formed by the alumina particles have edges with extruded platelets.[14] The observation of a protruding hard phase under one set of erosion conditions and recessed hard phase under another set of condition have been observed by other researchers.[25–27] The protruding hard phase is associated with a reduced erosion rate for the composite (or cast iron) relative to the unreinforced matrix, while the recessed hard phase is associated with an increased erosion rate relative to the unreinforced matrix material.[25–27]

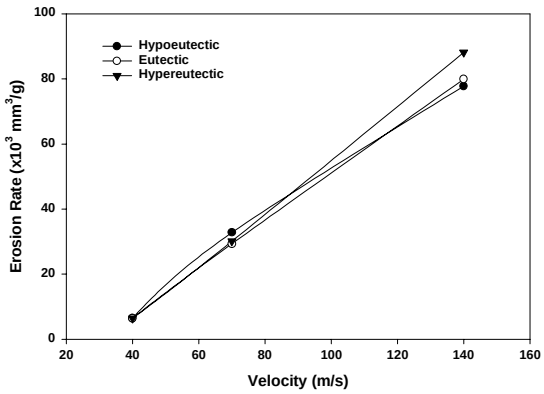


**Fig. 9. Erosion rates of white cast irons as a function of particle velocity.**

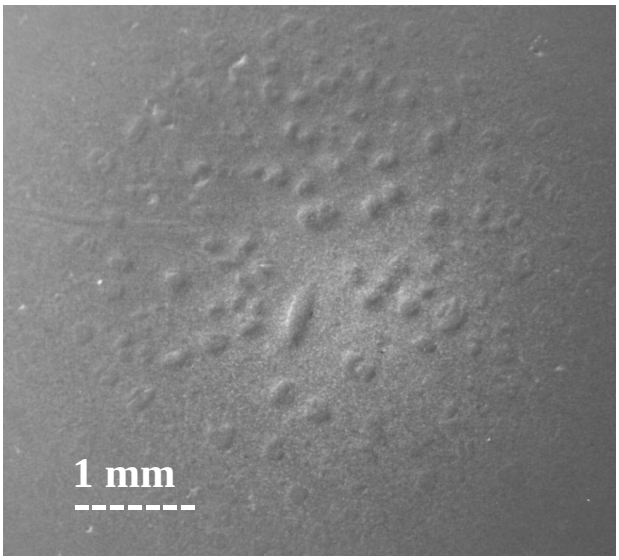


**Fig. 10. Erosion damage inside the erosion crater of hypereutectic white cast iron after testing at 40 m/s.**

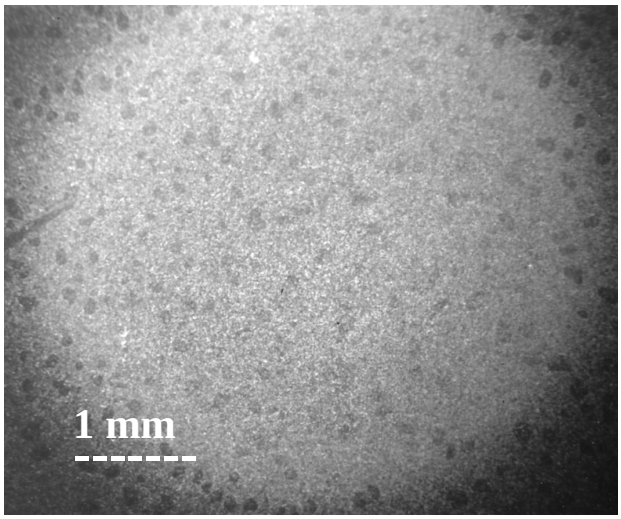


**Fig. 11. Erosion damage inside the erosion crater of hypereutectic white cast iron after testing at 140 m/s.**

The results of the jet erosion test on the as cast and heat treated Cr/TiC steels, 440C steels, and TiC particle reinforced P/M composites are summarized in Fig. 12. In this figure, the erosion rate is graphed as a function of hardness. Two features stand out. First, the erosion rate of the as-cast 440C is very good given its low hardness. Second, the erosion rates of the TiC particle reinforced P/M composites are not very good given their high hardness. These trends are consistent with a number of other studies. For most methods used to strengthen metals, the erosion rate increases or remains the same as the strength (and hardness) increases.[1, 24–32]

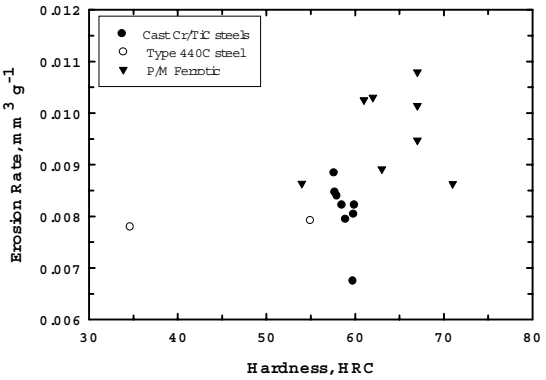


**Fig. 12. Erosion rates of Cr/TiC steels, 440C steels, and TiC particle reinforced P/M composites.**

## CONCLUSIONS

Several trends due to material properties and erosive conditions have been observed in the erosion rates of the materials tested in this study. The erosion rate of WC-Co cemented carbides decreased as the interparticle spacing decreased. Hard reinforcing phases of WC and $TiB_2$ provide more erosion resistance than TiC in FeAl matrix cermets. It appears that oxidation did not degrade the erosion resistance of FeAl-cermets, while oxidation degraded the erosion resistance of WC-Co cemented carbides. At relatively low velocities, the carbides in the white cast irons are more erosion resistant than the matrix, while at higher velocities the matrix is more erosion resistant.

## REFERENCES

1. G. Sundararajan and M. Roy, Tribology International, 30 (1997) 340–359.
2. J. R. Nicholls, Materials at High Temperatures, 14 (1997) 289–306.
3. G. Wright, Materials Science and Engineering, 88 (1987) 261–271.
4. D. E. Alman, J. H. Tylczak, J. A. Hawk, and J. H. Schneibel, submitted to Materials Science and Engineering, A.
5. J. H. Schneibel, C. A. Carmichael, C. A. Specht, and E. D. Subramanian, in Sintering Technologies, eds. R. M. German, G. L. Messing, and R. G. Cornwall, Marcel Dekker, NY, 1995, p. 253.
6. T. N. Tiegs, K. B. Alexander, K. P. Plucknett, P. A. Menchhofer, P. F. Becher, and S. B. Waters, Materials Science and Engineering, A209 (1996) 243.
7. R. Subrumanian, J. H. Schneibel, K. B. Alexander and K. P. Plucknett, Scripta Materialia, 35 (1996) 583.
8. R. Subrumanian, J. H. Schneibel, Intermetallics, 5 (1997) 401.
9. D. E. Alman, J. A. Hawk, J. H. Tylczak, C. P. Doğan, and R. D. Wilson, submitted to Wear of Materials 2001.
10. D. E. Alman, J. H. Tylczak, J. A. Hawk, and M. G. Hebsur, Materials Science and Engineering, A261 (1999) 245–251.
11. M. G. Hebsur, Materials Science and Engineering, A261 (1999) 24–37.

12. M. G. Hebsur, in J. A. Graves, R. R. Bowman, J. J. Lewandowski (eds.), Intermetallic Matrix CompositesBIII. Materials Research Society Symposium Proc. Vol. 350, Materials Research Society, Pittsburgh, PA, 1994, pp.177–182.
13. Ö. N. Doğan, J. A. Hawk, G. Laird II, Metallurgical and Materials Transactions 28A (1997) 1315–1328.
14. Thomas A. Adler and Ö. N. Doğan, Wear, 225–229 (1999) 174–180.
15. Ö. N. Doğan, J. A. Hawk and J. H. Tylczak, submitted to Wear of Materials 2001.
16. ASTM, Conducting erosion tests by solid particle impingement using gas jets, G 76–95, Vol. 03.02, Annual Book of ASTM Standards, American Society of Testing and Materials, Philadelphia, PA, 1996.
17. K. Anand and H. Conrad, Journal of Materials Science, 23 (1988) 2931–2942.
18. K. Anand and H. Conrad, Materials Science and Engineering, A105/106 (1988) 411–421.
19. K. Anand and H. Conrad, in Wear of Materials—1987, K. C. Ludema (ed.), ASME, NY (1987) pp. 135–142.
20. M. K. Keshavan and N. Jee, Metal Powder Report, 42 (1987) 86–869.
21. S. D. F. Wayne, J. B. Baldoni, and S.-T. Buljan, Tribology Transactions, 33 (1990) 611–617.
22. R. C. Pennefather, S. E. Hankey, R Hutchings and A. Ball, Materials Science and Engineering, A105/106 (1988) 389–394.
23. J. Ninham and A. V. Levy, Wear, 121 (1988) 347–361.
24. Ninham, Wear, 121 (1998) 307–324.
25. S. S. Aptekar and T. H. Kosel, in Wear of Materials—1985, K. C. Ludema (ed.), American Society of Mechanical Engineers, New York, NY (1985) pp. 677–686.
26. T. H. Kosel and S. S. Aptekar, Corrosion =86, NACE, Houston, TX (1986), Paper 113.
27. S. Seetharamu, P Sampathkumaran, and R, K. Kumar, Wear 186–187 (1995) 159–167.
28. J. S. Hansen, in Erosion: Prevention and Useful Applications, ASTM STP 664 (1979) pp. 148–162.
29. L. P. McCabe, G. A. Sargent, H. Conrad, Wear, 105 (1985) 257–277.
30. S. Srinivasan, R. O. Scattergood, and R. Warren, Metallurgical Transactions, 19A (1988) 1785–1793.
31. M. Hutchings and A. V. Levy, Wear, 131 (1989) 105–121.
32. F. Levin, J. N. DuPont, and A. R. Marder, Wear, 238 (2000) 160–167.